DEPARTMENT OF PHYSICS, UNIVERSITY OF JYVÄSKYLÄ
RESEARCH REPORT No. 3/1997

# ONE DIMENSIONAL ARRAYS OF SMALL NORMAL METAL TUNNEL JUNCTIONS AS THERMOMETERS AND SINGLE CHARGE PUMPS

**BY**
**KARI HIRVI**

Academic Dissertation
for the Degree of
Doctor of Philosophy

Jyväskylä, Finland
June 1997

URN:ISBN:978-951-39-9589-8
ISBN 978-951-39-9589-8 (PDF)
ISSN 0075-465X

Jyväskylän yliopisto, 2023

ISBN 951-34-0977-5
ISSN 0075-465X

DEPARTMENT OF PHYSICS, UNIVERSITY OF JYVÄSKYLÄ
RESEARCH REPORT No. 3/1997

# ONE DIMENSIONAL ARRAYS OF SMALL NORMAL METAL TUNNEL JUNCTIONS AS THERMOMETERS AND SINGLE CHARGE PUMPS

BY
KARI HIRVI

Academic Dissertation
for the Degree of
Doctor of Philosophy

To be presented, by permission of the
Faculty of Mathematics and Natural Sciences
of the University of Jyväskylä,
for public examination in Auditorium FYS-1 of the
University of Jyväskylä on June 13, 1997
at 12 o'clock noon

Jyväskylä, Finland
May 1997

## PREFACE

This work has been carried out during 1994-1997 at the University of Jyväskylä, Department of Physics. I wish to express my gratitude to my main supervisor Jukka Pekola and also Mikko Paalanen, who helped me in the begining before moving to Helsinki University of Technology. All the regular and visiting members of our research group are thanked for pleasant collaboration.

I would like to thank the staff of our Department of Physics.

The Academy of Finland is gratefully acknowledged for supporting me during my thesis work.

# Contents

1 Introduction 4

2 Arrays of tunnel junctions 5
2.1 General discussion . . . . . 5
2.2 Coulomb blockade . . . . . 6
2.3 Thermometry by arrays of tunnel junctions . . . . . 8
2.3.1 Basic results . . . . . 8
2.3.2 Higher order corrections to the basic result . . . . . 11
2.3.3 Inhomogeneities in the array . . . . . 12
2.3.4 Background charges . . . . . 15
2.4 Computational methods . . . . . 16
2.4.1 The $IV$ - curve of a 2 - junction array: an iterative algorithm . . . . . 16
2.4.2 The $IV$ - curve of an $N$ - junction array: principle of the numerical simulation . . . . . 19
2.4.3 A practical method to extract $V_{1/2}$ from the conductance data . . . . . 23
2.5 Experimental results . . . . . 25
2.5.1 Fabrication and measurements . . . . . 25
2.5.2 Physical limitations . . . . . 25
2.5.3 Solitary junctions . . . . . 28
2.6 Pumping single electrons by surface acoustic waves . . . . . 30
2.6.1 Controlling single charges: metrological applications . . 30
2.6.2 SAW pump . . . . . 31

3 Publications 33

4 The author's contribution 35

# 1 Introduction

In the last decade interest in physics of small, submicrometer scale metal-oxide-metal tunnel junctions and advanced fabrication technology led to the observation of single particle, namely electron, tunnelling.

The ability to move electrons one at a time has inspired attempts to use it, e.g., for metrological applications for constructing a standard for current based on microscopic foundation [1, 2, 3]. One would force electrons to travel through an array of tunnel junctions one by one at a frequency $f$, resulting in current $I$ determined by the frequency and the elementary charge[1] $e$ as $I = ef$. Another possible application of this so called single electronics would be to use single electrons to store information, i.e., to represent bits of computer memory or logic states by presence or absence of just one electron [4, 5, 6, 7]. Two tunnel junctions in series with a gate electrode form a single electron transistor (SET), which can be used as a very sensitive electrometer [8, 9, 10, 11].

The natural energy scale of single electron systems is $E_C = e^2/2C$, where $C$ is the geometrical capacitance of the metal-oxide-metal junction and $E_C$ is the energy of one electron charging the capacitor plates, i.e., the energy required for tunnelling. In the above mentioned applications, the charging energy $E_C$ must be much higher than the thermal energy $k_BT$, or otherwise thermal fluctuations will smear out single charge phenomena. Therefore, effort has been mostly focused to this regime, $E_C \gg k_BT$, whereas the opposite high temperature limit, $E_C < k_BT$, has been largely overlooked. However, in this thesis it is demonstrated that there is interesting physics in the high temperature limit also, and, astonishingly, we provide the first commercially potential application of single electron tunnelling research: thermometry. When the thermal energy, $k_BT$, is higher or comparable to the charging energy, $E_C < k_BT$, the conductance vs. bias voltage curve of an array of tunnel junctions exhibits features suitable for primary thermometry. The curve represents a nearly bell shaped dip in conductance whose half width, $V_{1/2}$, is directly proportional to absolute temperature. We have found out that the tunnel junction thermometer is also quite robust to fabrication inhomogeneities, background charges and external magnetic field. Usable temperature range for AlOx based tunnel junctions presently ranges from 10 mK up to 77 K. Since one is usually interested in the temperature of the lattice rather than that of the electrons, poor electron-phonon coupling becomes the limiting factor at low temperatures. At high temperatures tunnel junction

[1] Let us use the convention $e > 0$.

barrier starts to deform due to the high bias voltage needed to measure the broad conductance dip and $V_{1/2}$.

# 2 Arrays of tunnel junctions

## 2.1 General discussion

The object of study in this thesis is a one dimensional array of $N$ tunnel junctions in series as depicted in Fig. 1. The junctions are made of two slightly overlapping metal layers separated by a thin oxide layer. The overlap and the oxide layer result in a capacitance $C_i$ and the resistance $R_{T,i}$ of a junction $i$, which is modeled by a parallel connection of $R_{T,i}$ and $C_i$. The junctions $i$ and $i+1$ isolate a small metallic island, which also has a stray capacitance $C_{0,i}$. Optionally, on each island $i$ one can attach a *gate*, which is simply a metallic lead manufactured near the island producing capacitance $C_{g,i}$ with island $i$. By applying a voltage $V_{g,i}$ to the gates through external wiring, one can *change* the potentials of the islands. This is discussed more in Sec. 2.6 where we concentrate on single charge transferring devices.

The arrays and junctions sit on an isolating substrate, e.g., silicon at low temperature. The capacitances between the non-adjacent islands are negligibly small. The array is biased symmetrically at the two ends by voltages $\pm V/2$ and one is usually interested in the current vs. voltage ($IV$) relationship of the array. Electrons tunnel through individual junctions yielding a net flow of charge through the array at nonzero bias voltage.

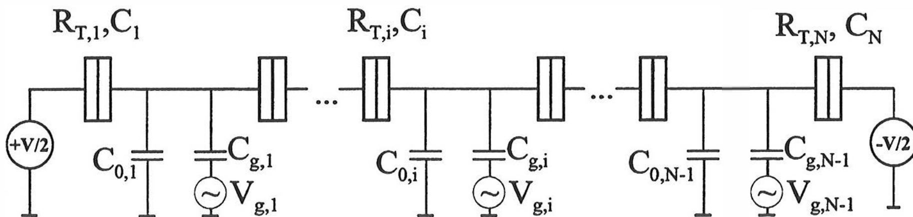


Figure 1: *A symmetrically biased one dimensional array with N tunnel junctions and N-1 stray capacitances $C_{0,i}$ included. $C_{g,i}$ and $V_{g,i}$ denote the gate capacitances and the gate voltages, respectively.*

There are up to billions of electrons on each island, and their charge is largely compensated by the lattice ions. Yet, due to the smallness of the islands, a lack or an excess of a *single* electron can change the electrostatic

energy of an array considerably. Thus, for the phenomena under study, the charge configuration $\{n\} \equiv \{n_1, n_2, \ldots, n_N\}$, describing the number of *excess* electrons on each island $i$, is sufficient to completely define the state of the array. Naturally, $n_i$ may have negative values and this means that there is a lack of electrons on island $i$.

Each configuration $\{n\}$ has a probability $\sigma(\{n\})$ of occuring, which depends on the absolute temperature $T$, the bias voltage $V$ and the parameters of the array introduced above. We limit ourselves to the tunnelling event between the adjacent islands $i$ and $i+1$, i.e., an electron can tunnel through just one junction at a time, and denote the tunnelling probability by $\Gamma_j^{\pm}(\{n\})$ through the junction $j$ at the state $\{n\}$ to the left (-) or right (+), respectively. Tunnelling through several junctions simultaneously, the so called co-tunnelling, yields small effects in short arrays ($N \cong 5$) at low temperatures [12, 13], but it is unimportant for the present discussion. The ends of the array are held at a constant potential regardless of tunnelling through the first/last junction. This means that we assume that the array is perfectly voltage biased.

The configuration probabilities $\sigma(\{n\})$ are determined by a master equation [14] which can be written for $N$ junctions as

$$\begin{aligned}\dot{\sigma}(\{n\}) = \textstyle\sum_j \{&\sigma(\ldots, n_j - 1, n_{j+1} + 1, \ldots)\Gamma_j^-(\ldots, n_j - 1, n_{j+1} + 1, \ldots) \\ &+\sigma(\ldots, n_j + 1, n_{j+1} - 1, \ldots)\Gamma_j^+(\ldots, n_j + 1, n_{j+1} - 1, \ldots) \\ &-[\Gamma_j^+(\ldots, n_j, n_{j+1}, \ldots) + \Gamma_j^-(\ldots, n_j, n_{j+1}, \ldots)]\sigma(\ldots, n_j, n_{j+1}, \ldots)\}.\end{aligned} \tag{1}$$

What is written in Eq. (1) is the probability flux into configuration $\{n\}$ minus the flux out of it. In steady state one has $\dot{\sigma}(\{n\}) = 0$, i.e, when there is no gate modulation or any other fluctuations in charge or voltage. The tunnelling probabilities $\Gamma_i^{\pm}$ depend on the electrostatic energy difference for the states before and after the tunnelling event [15].

## 2.2 Coulomb blockade

Let us study a perfectly symmetric two junction case ($N = 2$) with a gate and ignore the ground capacitance for simplicity. Furthermore, we assume that temperature is low, i.e., $E_C \gg k_B T$. The center island has a capacitance $C_\Sigma = 2C + C_g$ with the environment and, thus, one additional electron on the island changes the energy by the amount $e^2/2C_\Sigma$. At low temperature and at low bias voltage, it may not be possible for an electron to tunnel into

the center island, i.e., the energy required to charge the island ($e^2/2C_\Sigma$) far exceeds the energy available either from thermal excitations ($k_BT$) or from the bias supply ($eV/2$), $e^2/2C_\Sigma \gg eV/2, k_BT$.

Once the flow of electrons is prohibited, one observes zero current at nonzero bias voltage in the $IV$ - curve of the array: a phenomenon called *Coulomb blockade.* Asymptotically, at high bias voltages, the $IV$ - curve approaches that of an ohmic resistor of resistance $2R_T$, but with an offset voltage $V_{off} = e/2C$. This model suggests that at zero temperature one would have a sharply defined threshold voltage $V_{off}$ for the onset of current, and absolutely no current when $|V| < V_{off}$. However, the co-tunnelling effects give rise to nonvanishing current even in the Coulomb blockade region, i.e., electrons tunnel through both junctions simultaneously with virtually no increase in charging energy. Also, we have neglected quantum fluctuations, which give rise to nonperfect Coulomb blockade. They can be effectively suppressed, however, by making the resistance of junctions, $R_{T,i}$, much higher than $R_K = h/e^2 \simeq 26\ k\Omega$.

The situation changes considerably by varying the gate (with capacitance $C_g$) voltage $V_g$. The electrostatic energy of the system is

$$E = (-ne + Q_g)^2/2C_\Sigma \; . \tag{2}$$

The charge induced by the gate voltage $V_g$ is $Q_g = C_gV_g$, and $n$ is the number of electrons on the island. Since $n$ can have only integer values, the corresponding change in $E$, $\Delta E$, determines the energy needed for an electron to tunnel into or out from the island initially in the state of minimum energy. Interestingly, one can change $\Delta E$ by varying the gate voltage $V_g$ and thus $Q_g$. Minimum $\Delta E = 0$ is achieved when $Q_g = (n \pm 0.5)e$ and the Coulomb blockade is almost nonexistent, i.e., the $IV$ curve follows closely to that of an ohmic curve. The gate controls the electrostatic energy barrier and has effect only at very low temperatures where thermal fluctuations are suppressed. The occupation of the island with $Q_g = 0$ consists mostly of states $n = 0, \pm 1$ and thus a change in $Q_g$ by a fraction of electron charge changes the current considerably. Gated two junction arrays can be used as very sensitive electrometers as demonstrated in Ref. [16] down to $< 10^{-4}\ e/\sqrt{Hz}$ noise level.

The models of Coulomb blockade and related experimental results are depicted by a series of pictures in Fig. 2.

Typical junction capacitances are of the order $C \sim 10^{-15} - 10^{-16}$ F which translates to temperature as $T \sim E_C/k_B \sim 1 - 10$ K. Temperature should

therefore be well below 1 K for Coulomb blockade to be clearly visible. Recently, however, Coulomb blockade has been demonstrated at much higher temperatures [17, 18, 19], in a special setup even up to room temperature [20]. Resistances of the junctions are typically $\geq 30$ k$\Omega$. Fabrication and further properties of the junctions are described in Sec. 2.5.

In summary, a tiny metal structure can have a capacitance with the environment small enough for the associated single electron charging energy to be decisive in its electrical behaviour, leading to nonlinear $IV$-characteristics with Coulomb blockade.

## 2.3 Thermometry by arrays of tunnel junctions

### 2.3.1 Basic results

The Coulomb blockade is dominant in the low temperature regime, $E_C \gg k_BT$, but there is also interesting physics in the opposite limit, $E_C \ll k_BT$, where charging energy is inferior but not insignificant as compared to $k_BT$. It was discovered in Ref. [P1] that, in the high temperature limit, arrays of normal metal tunnel junctions exhibit features suitable for *primary thermometry.* The thermometer operation is based on the universal shape of the conductance curve of the array.

For an gateless $N$ - junction array, let us define dimensionless parameters $u_N \equiv 2\frac{N-1}{N}\frac{E_C}{k_BT}$ for the absolute temperature $T$ and $v_N = eV/Nk_BT$ for the bias voltage $V$. Assuming that there are no ground capacitances[2] , $C_{0,i} \equiv 0$, and the array is symmetric, $R_T \equiv R_{T,i}$ and $C \equiv C_i$ (Fig. 1), the conductance $G$ normalized by its asymptotic value, $G_T$, at $v_N \to \pm\infty$, is given by

$$\frac{G(v_N)}{G_T} = 1 - u_N g(v_N) , \tag{3}$$

where the function $g$, introduced in [P1], is defined by

$$g(x) = [x \sinh(x) - 4\sinh^2(x/2)]/8\sinh^4(x/2). \tag{4}$$

Equation (3), strictly valid only when $E_C \ll k_BT$, represents a dip in conductance as shown in Fig. 3. The full width at half minimum, $V_{1/2}$, and the normalized depth of the peak, $\Delta G/G_T$, are given by

[2]In practise the ground capacitances can be neglected in most cases.

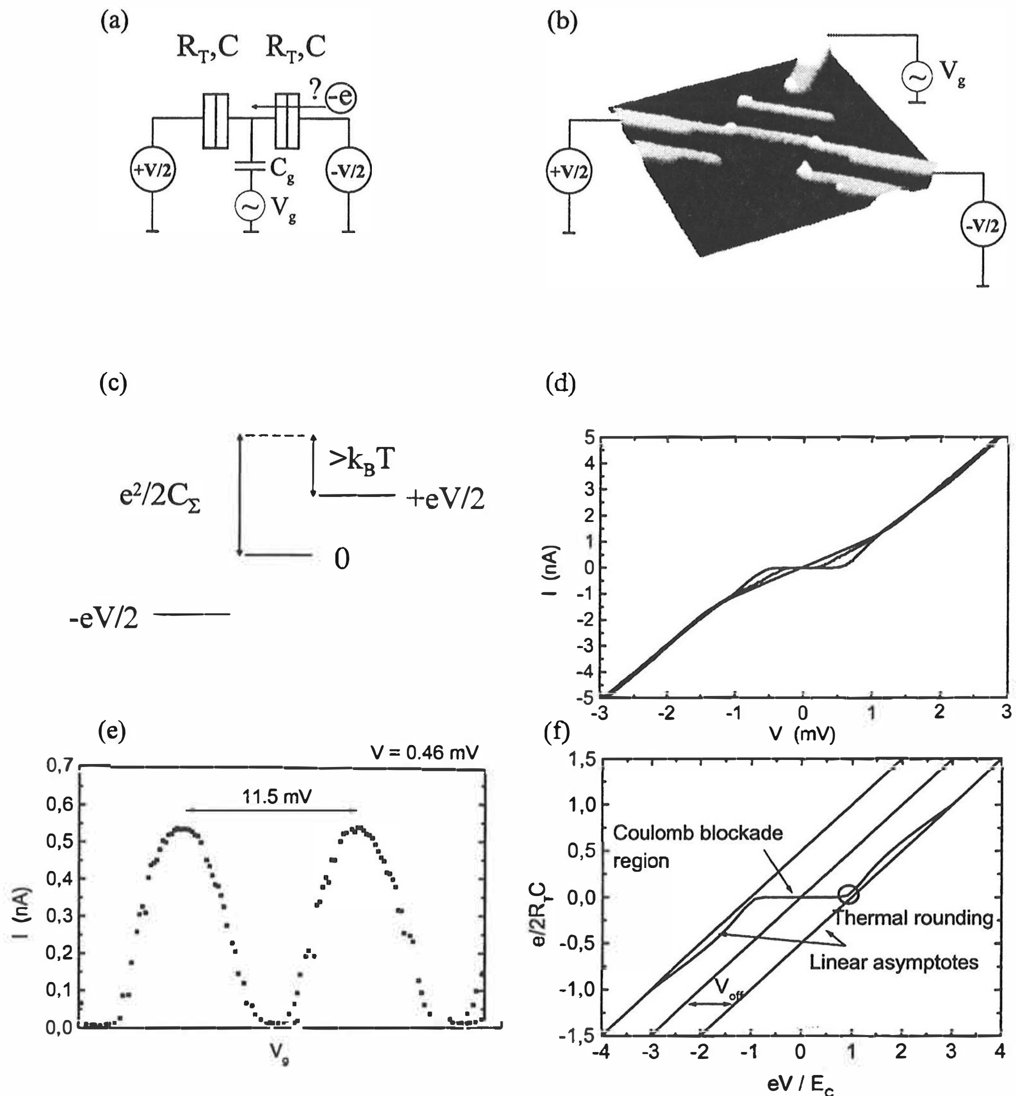


Figure 2: *Operation of a symmetrically biased SET transistor. (a) A schematic picture of the experimental setup and (b) an atomic force microscope (AFM) image of the actual transistor. The overlapping white areas are the tunnel junctions. (c) The potentials felt by a single electron with negligible charging energy of the island (solid line) and with the charging energy included (dashed line). The electron prefers not to move onto the island unless it gains enough energy from the voltage supply or from thermal excitations to win the charging energy. (d) Measured IV characteristics of a transistor with* $R_T \simeq 200\ k\Omega$, $C_\Sigma = 2.0 \cdot 10^{-16}\ F$ *at* $T = 100\ mK$ *for different gate voltages and (e) modulation of current of the same transistor at a fixed bias voltage as the gate voltage is varied. (f) Calculated current vs. voltage (IV) relationship (solid line) at a low temperature* $(e^2/2C)/(k_BT) = 40$. *Coulomb blockade is clearly manifested as a flat zero current region at voltages below* $|eV/E_C| \simeq 1$. *The IV - curve becomes linear as* $V \longrightarrow \pm\infty$. *At nonzero temperature there is thermal rounding of the IV - curve at the onset of current at the voltages* $|V| \simeq V_{off} = e/2C$.

$$V_{1/2} \simeq 5.44\frac{Nk_BT}{e} \tag{5}$$

$$\frac{\Delta G}{G_T} = \frac{u_N}{6} = \frac{N-1}{3N}\frac{e^2/2C}{k_BT}. \tag{6}$$

For a given array of length $N$, the half width (Eq. (5)) is directly proportional to temperature $T$ and, since it depends only on the fundamental constants of nature, is a *primary* measure of $T$. The depth of the peak (Eq. (6)) gives us a *secondary* thermometric parameter, since at least one calibration point is needed for the capacitance $C$. The factor '5.44', in fact 5.43917..., comes from the numerical solution of Eq. (3) for the half width, and it simply yields one characteristic measure to extract $T$ directly.

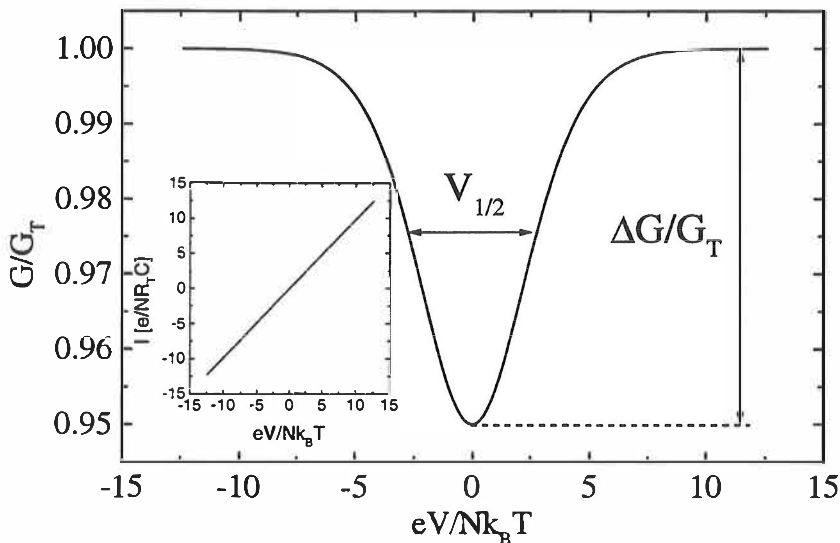


Figure 3: *Conductance in the high temperature regime from Eq. (3) for* $u_N = 0.30$. *The inset contains the corresponding IV - curve, from which the weak Coulomb blockade is not easily seen, as contrasted to the low temperature case in Fig. 2 (with N=2).*

As indicated by the $IV$ - curve in the inset of Fig. 3, the Coulomb blockade tendency is quite weak. Therefore, in the experiment, instead of measuring the $IV$ - curve and numerically differentiating it, one measures the conductance directly using standard lock-in techniques for much greater accuracy.

In principle, the absolute temperature $T$ by itself has little meaning as far as the Coulomb blockade is concerned. Instead, one must always compare the thermal energy $k_B T$ to the characteristic energy $E_C$ of the array. Therefore for a given temperature range, one can experimentally 'tune' the array by varying the size, i.e., the capacitance $C$, of the junctions. By lock-in techniques one can measure conductance minima at $\Delta G/G_T = 0.2\%$ and the Coulomb blockade is not yet approached when $\Delta G/G_T = 30\%$. This gives the ratio of the maximum and the minimum measurable temperatures $T_{max}/T_{min} \sim 100$ by just one array, where the mean of the temperature range, $T_{mean}$, is determined by the capacitances of the array. There are, however, some limitations. Increasing $E_C$ increases $T_{mean}$ but also the conductance dip widens and one has to use large bias voltages to measure the dip. Large bias tends to distort the apparent potential barrier of the junctions which shows as deviations from the simple theory. This effect limits the use of the aluminium based tunnel junction thermometer to temperatures up to $T \approx 77$ K at present.

### 2.3.2 Higher order corrections to the basic result

Actually, the results in Sec. 2.3.1 are correct only up to the first order in $u_N$. As the temperature is lowered, higher order terms in conductance become noticeable. In Ref. [P2], the master equation (Eq. (1)) was solved and a general formula for the conductance of a symmetric array ($R_{T,i} \equiv R_T, C_i \equiv C, C_{0,i} \equiv 0$) was derived :

$$\begin{aligned}\frac{G(v_N)}{G_T} &= 1 - u_N g(v_N) - \frac{1}{4}u_N^2\left[g''(v_N)h(v_N) + g'(v_N)h'(v_N)\right] \\ &\quad -\frac{1}{8}u_N^3\left[\frac{1}{4}g^{(4)}(v_N)h(v_N)^2 + \frac{1}{3}g''(v_N) + \frac{1}{2}g'''(v_N)h'(v_N)h(v_N)\right] \\ &\quad -\frac{1}{16}u_N^4\left[\frac{1}{6}g^{(4)}(v_N)h(v_N) + \frac{1}{6}g'''(v_N)h'(v_N) + \frac{1}{8}g^{(5)}(v_N)h(v_N)^2h'(v_N)\right. \\ &\quad\quad \left. + \frac{1}{24}g^{(6)}(v_N)h(v_N)^3\right] + O(u_N^5)\end{aligned} \tag{7}$$

with $h(x) = x\coth(x/2)$.

Similarly at $v_N = 0$, one obtains the depth of the peak as

$$\frac{\Delta G}{G_T} = \frac{1}{6}u_N - \frac{1}{60}u_N^2 + \frac{1}{630}u_N^3 - \frac{1}{5040}u_N^4 + O(u_N^5) \tag{8}$$

As a special case, Eqs. (7) and (8) are valid for an array of two tunnel junctions ($N = 2$). But for the two junction case one has a rigorous numerical method [P1], (Sec. 2.4.1) for calculating the $IV$ - curve, from which the conductance can be obtained as a numerical derivative. In $u_N, v_N$ units, the results for all $N$ are the same. Therefore, one has two different ways of calculating the conductance of an array with $N$ tunnel junctions.

Using the series expansions, one can calculate the linear correction to the ideal first order result [Eqs. (3), (5)]

$$\frac{\Delta V_{1/2}}{V_{1/2,0}} \simeq 0.39211 \frac{\Delta G}{G_T}, \tag{9}$$

where $V_{1/2,0}$ is full width at half minimum from Eq. (3) and $\Delta G/G_T$ is the exact (measured) depth of the peaks. Equation (9) is calculated from Eq. (7) using the terms up to the second order in $u_N$ and taking the first, i.e., linear, term of the series expansion of the correction formula. Figure 4 depicts corrections numerically calculated from Eq. (7) using terms up to the 2nd, 3rd and 4th order, as well as the correction using the rigorous method (Sec. 2.4.1) and the linear correction of Eq. (9).

The linear correction is seen to be quite accurate even up to such a high peak depth as $\Delta G/G_T = 0.3$. Since Eq. (9) was calculated using the terms up to $u_N^2$, this might suggest that including the second order term is sufficient for describing the *whole* conductance dip. This is, however, not true for deep peaks, as shown by a series of pictures for various peak depths in Fig. 5. The fact that the linear correction applies so well up to high values of $\Delta G/G_T$ is presumably a lucky coincidence.

### 2.3.3 Inhomogeneities in the array

Inevitably, there are some inhomogeneities in the tunnel junction parameters $R_{T,i}, C_i$ and $C_{0,i}$ due to the fabrication process. To study the effect of nonideal circumstances, we first draw upon the first order result for the conductance in the case of nonequal resistances and capacitances [P3]

$$\frac{G}{G_T} = 1 - 2\sum_{i=1}^{N} \frac{R_{T,i}}{R_\Sigma} \frac{\Delta_i}{k_B T} g\left(\frac{R_{T,i}}{R_\Sigma} \frac{eV}{k_B T}\right) \tag{10}$$

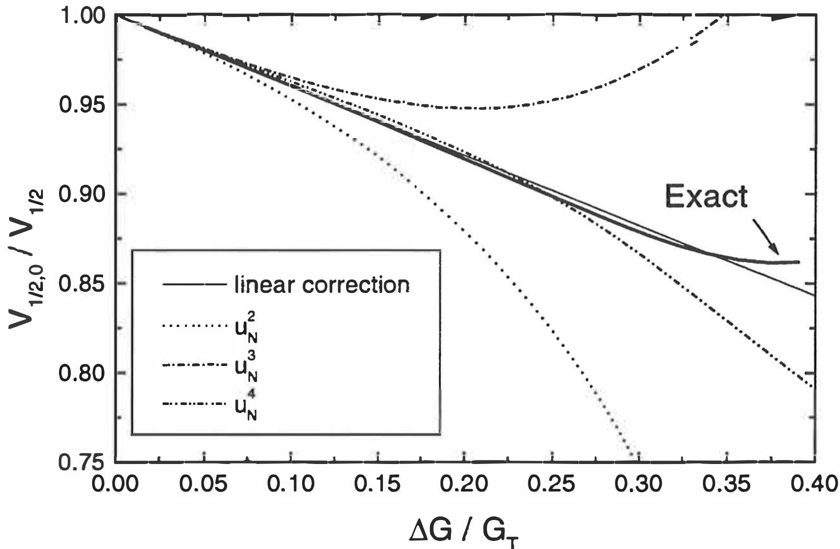


Figure 4: *Corrections to the first order half width of Eq. (3), now denoted by $V_{1/2,0}$, as calculated up to various orders in $u_N$. The linear correction and the one from the rigorous calculation ('exact') follow each other quite nicely. $\Delta G/G_T$ is the true depth of the peak.*

where $R_\Sigma$ is the total resistance, $R_\Sigma = \sum_{i=1}^{N} R_{T,i}$ and $\Delta_i$ describes the Coulomb blockade threshold for the junction $i$. The term $\Delta_i$ is given by the inverse capacitance matrix $\mathbf{C}^{-1}$ of the array: $\Delta_i = (\mathbf{C}^{-1}_{i-1,i-1} + \mathbf{C}^{-1}_{i,i} - 2\mathbf{C}^{-1}_{i,i-1})e^2/2$. If there are variations in the capacitances $C_i$ and $C_{0,i}$, but the resistances are equal $R_{T,i} = R_\Sigma/N$, Eq. (10) reduces to

$$\frac{G}{G_T} = 1 - 2 \cdot \frac{\sum_{i=1}^{N} \Delta_i}{N k_B T} \cdot g(\frac{eV}{N k_B T}), \tag{11}$$

which has exactly the form of Eq. (3) with $u_N$ replaced by $2\sum_{i=1}^{N} \Delta_i / N k_B T$; the two quantities coincide for a homogeneous array. Therefore Eq. (5) is valid for the half width always if the resistances $R_{T,i}$ are equal even if capacitances would be different from each other. On the other hand, nonequal resistances cause deviations from Eq. (5) and one can use Eq. (10) to calculate the full curve and the half width, or use the following correction formula.

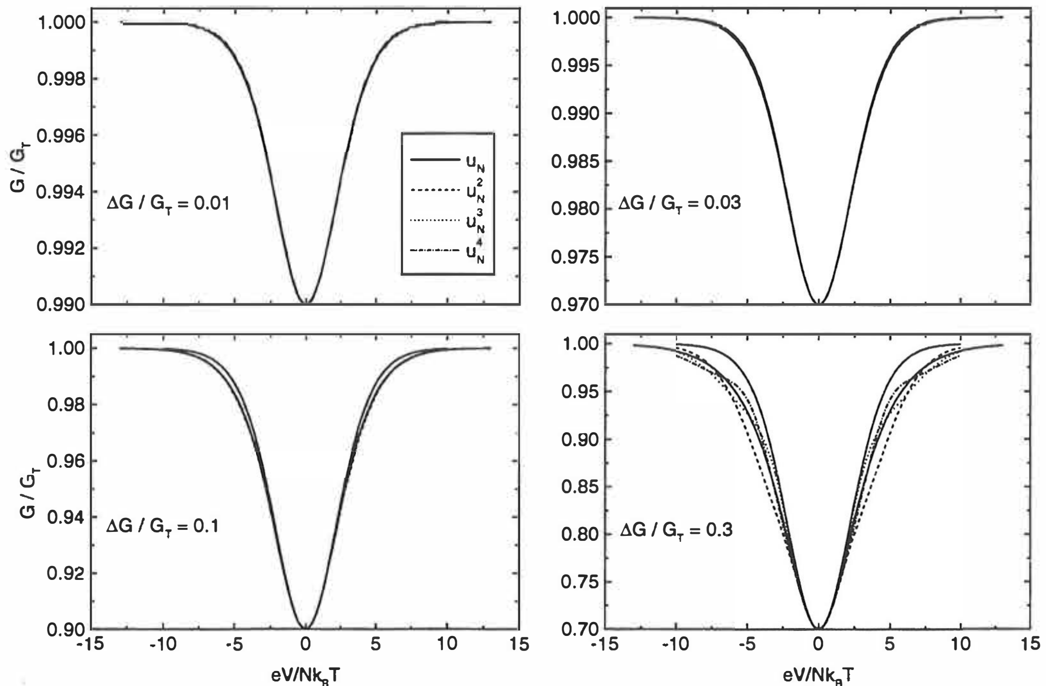


Figure 5: *Four peaks with increasing depth as calculated from Eq. (7) up to different orders in $u_N$. The solid line which extends further in bias than all the others, is from the rigorous calculation, i.e., the one against which the other curves from the series expansion are to be compared.*

If we assume uniform thickness of the tunnel junction barrier (uniform oxidation) it is supposed that $R_{T,i}C_i = constant$ for all junctions, since $R_{T,i} \propto A_i^{-1}$ and $C_i \propto A_i$, where $A_i$ denotes the tunnelling area of junction $i$. In the case of small variations and for $R_{T,i}C_i = constant$, the dependence of $V_{1/2}$ on the variations is of quadratic form

$$\frac{V_{1/2}}{V_{1/2,0}} \approx 1 - k \left(\frac{\delta R}{R_0}\right)^2_{RMS}, \tag{12}$$

where $(\delta R/R_0)^2_{RMS}$ is the RMS deviation of junction resistances from their mean value $R_0 = R_\Sigma/N$. The factor $k$ has an approximate value of $k \cong 0.73 + (N-1)/N$ [P3] and the half width for the homogeneous case from Eq. (5) is $V_{1/2,0}$.

Inhomogeneities were studied experimentally in Ref. [P3] and by computer simulations in Ref. [P4]. Both methods confirm a weak dependence of $V_{1/2}$ on the inhomogeneities. The ratio of the maximum and minimum areas of junctions within a chain could be as high as $A_{max}/A_{min} = 10$ and yet only a factor of 2 drop of $V_{1/2}$ was observed [P3]. A 10% peak-to-peak variation in sizes of junctions yields an error of about 0.2% in $V_{1/2}$ and $T$. The effect of inhomogeneities in the junction parameters is easy to push down to below 1% level in error, in arrays where the junctions are not pushed to the minimum size.

### 2.3.4 Background charges

The effect of variations in the junction parameters ($R_{T,i}$ and $C_i$) could be calculated analytically in the high $T$ limit, but to account for background charges one has to resort to numerical simulations. Background charges are highly uncontrollable in the experiment and arise from the intrinsic properties of the materials used, whereas $R_{T,i}, C_i$ variations are attributed to the fabrication errors of the arrays.

On each island a random offset charge $q_{0,i}$ was introduced drawn from a uniform distribution within the interval $[-e/2, +e/2]$, since the effect of background charges $q_{0,i}$ is $e$ periodic. The uniform distribution reflects the fact that nothing is known about $q_{0,i}$'s, i.e., there is no reason to prefer some charges over the other. Some simulations were performed with a uniform nonzero background charge $q_0 \equiv q_{0,i}$, with results equal to those in the other configurations in the high temperature limit.

The effect of background charges on $V_{1/2}$ and $\Delta G/G_T$ are shown in Fig. 6 for arrays of 10 and 40 junctions as a function of $u_N$, i.e., against $T$. The two junction case was studied in Ref. [P1]. It is seen that the correction to the first order half width $V_{1/2,0}$ is linear in the beginning and that the background charges start to have noticeable effect only as the temperature is lowered such that $u_N > 3$. This insensitivity to $q_{0,i}$ can be qualitatively explained by considering the number of electrons $n_i$ on each island $i$. At high temperatures, large ($\gg 1$) fluctuations of $n_i$ effectively mask the small offset charge $|q_{0,i}| \leq e/2$, i.e., the effect of the background charges is buried under the thermal noise and the offset charges start to have effect only when they become comparable to the fluctuations.

Devices built out of tunnel junction arrays that manipulate charges at *single* electron level are always hampered by background charge problems. But in the thermometric operation we are not addressing single electrons and the natural high temperature operating regime is much more forgiving

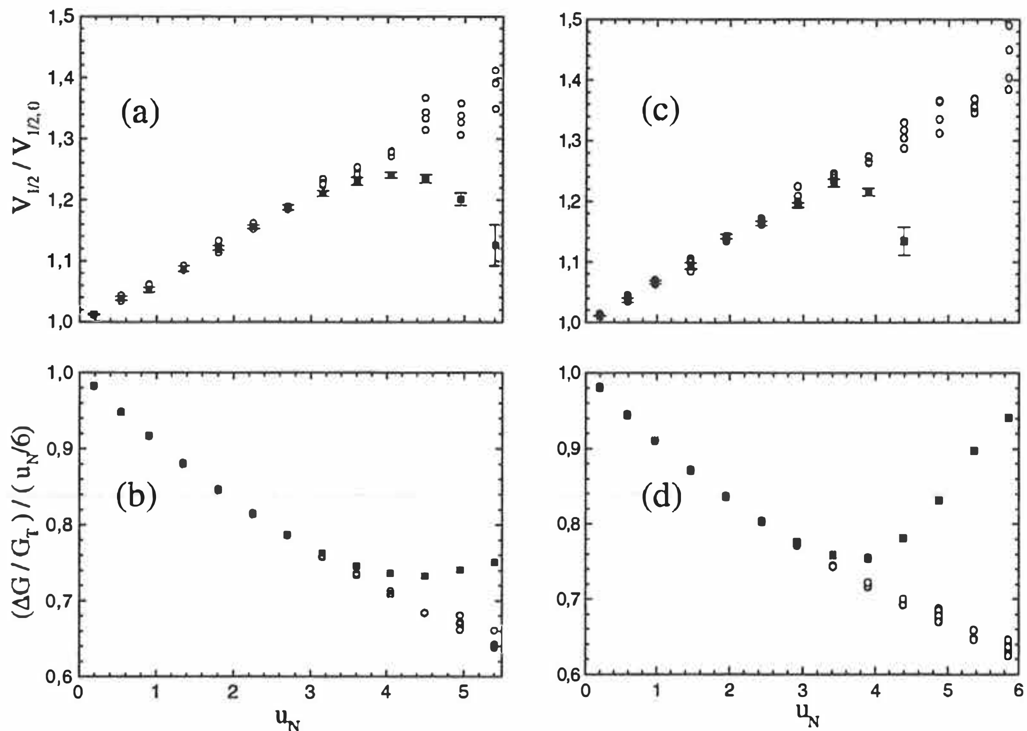


Figure 6: *Background charge effects on $V_{1/2}$ and $\Delta G/G_T$ for (a),(b) 10 and (c),(d) 40 junctions vs. $u_N = 2((N-1)/N)(e^2/k_BT)$. Each point depicted by a circle was calculated with a different set of random background charges $\{q_{0,i}\}$ (see text). The homogeneous case ($R_{T,i}, C_i$ constant, $C_{0,i} = 0, q_{0,i} = 0$) is plotted with solid square symbols.*

in terms of the background charges.

## 2.4 Computational methods

### 2.4.1 The $IV$ - curve of a 2 - junction array: an iterative algorithm

In the symmetric, fully homogeneous case, we can calculate the $IV$ - curve of a two junction array ($N = 2$ in Fig. 1 without gates but possibly with the ground capacitance $C_0$) by a rigorous numerical method. The island between two junctions has a probability $\sigma(n)$ of occupying $n$ electrons. Due to symmetry, it is obvious that $\sigma(n) = \sigma(-n)$, i.e., "holes" and electrons have an equal probability of existing. Before proceeding, let us define

$$P_n \equiv \frac{\sigma(n+1)}{\sigma(n)} = \frac{\sigma(-(n+1))}{\sigma(-n)}$$

describing the ratio of the occupation probabilities of the adjacent charge states of the array.

In a steady state, $\dot{\sigma}(n) = 0$, and it directly follows from the master equation [Eq. (1)] that

$$\frac{A_n}{P_{n-1}} + B_n P_n - C_n = 0, \tag{13}$$

where we have introduced the notation

$$\begin{aligned} A_n &= \Gamma_1^+(n-1) + \Gamma_2^-(n-1) \\ B_n &= \Gamma_1^-(n+1) + \Gamma_2^+(n+1) \\ C_n &= \Gamma_1^+(n) + \Gamma_1^-(n) + \Gamma_2^+(n) + \Gamma_2^-(n). \end{aligned}$$

The tunnelling probabilities $\Gamma_{1,2}^{\pm}$ depend on $V, T$ and $n$. Using the normalization introduced before, we take the following shorthand notation $u \equiv e^2/(2C + C_0)/k_B T$ and $v \equiv v_2 = eV/2k_B T$ to account for temperature and bias[3]. Now the gammas are expressed as

$$\begin{aligned} \Gamma_1^{\pm}(n) &= \frac{1}{2R_T C} \frac{k_B T}{E_C} \frac{(-\frac{1}{2} \mp n)u \mp v}{1 - \exp([\frac{1}{2} \pm n]u \pm v)} \\ \Gamma_2^{\pm}(n) &= \frac{1}{2R_T C} \frac{k_B T}{E_C} \frac{(-\frac{1}{2} \pm n)u \mp v}{1 - \exp([\frac{1}{2} \mp n]u \pm v)}. \end{aligned}$$

When $n = 0$, it follows from Eq. (13) that

$$P_0 = \frac{C_0}{A_0 + B_0}. \tag{14}$$

From Eq. (13) one obtains a recursive formula for $P_n$ :

[3]Note that $u = u_2$ if the stray capacitance $C_0 = 0$.

$$P_n = \frac{C_n - (A_n/P_{n-1})}{B_n}. \qquad (15)$$

Next we calculate the ratio $\Upsilon_n$ between the probabilities $\sigma(n)$ and $\sigma(0)$ as

$$\Upsilon_n \equiv \frac{\sigma(n)}{\sigma(0)} = P_{n-1}\Upsilon_{n-1} \qquad (16)$$

and use the fact that $\sigma(n) = \sigma(-n)$ and normalize $\sum_{n=-\infty}^{n=\infty} \sigma(n) = 1$ to obtain an equation for the probability of a neutral state:

$$\sigma(0) = \left[1 + 2\sum_{n=1}^{\infty} \Upsilon_n\right]^{-1}. \qquad (17)$$

Now we are ready to give an algorithm for calculating the current at *any* temperature and biased at any voltage. First, the occupation probabilities $\sigma(n)$ are calculated up to a predefined maximum occupation $n_{max}$ for positive $n > 0$, after which the current is easily calculated as the weighted difference between the tunnelling rates at different occupations.

1. Calculate $P_0$ by Eq. (14) and set $n = 1$ and $\Upsilon_0 = 1$.
2. Calculate $P_n$ using $P_{n-1}$ (Eq. (15)).
3. Calculate $\Upsilon_n$ using $\Upsilon_{n-1}$ (Eq. (16)).
4. Advance to the next state, i.e., $n \longrightarrow n+1$ and go to step 2 if $n \leq n_{max}$.
5. Calculate $\sigma(0)$ from Eq. (17) by taking the sum up to $n = n_{max}$. The probabilities $\sigma(n)$ are now obtained (Eq. (16)) as $\sigma(n) = \sigma(0)\Upsilon_n$.
6. In equilibrium, the current through both of the junctions is the same, and thus it suffices to calculate the current through the first junction :

$$\begin{aligned} I &= -e \sum_{n=-\infty}^{\infty} \sigma(n) \left[\Gamma_1^+(n) - \Gamma_1^-(n)\right] \\ &\simeq -e \Big\{\sigma(0) \left[\Gamma_1^+(0) - \Gamma_1^-(0)\right] \\ &\quad + \sum_{n=1}^{n_{max}} \sigma(n) \left[\Gamma_1^+(n) - \Gamma_1^-(n) + \Gamma_1^+(-n) - \Gamma_1^-(-n)\right]\Big\} \end{aligned}$$

Conductance can be obtained by numerically differentiating the $IV$ - curve.

### 2.4.2 The $IV$ - curve of an $N$ - junction array: principle of the numerical simulation

We start the discussion of an $N$ junction array with some physical considerations to justify the simulation method to be described. Only the tunnelling events between the neighbouring islands are taken into account and single electrons are allowed to tunnel at a time. We recall that the effect of higher order cotunnelling processes is negligible for long arrays [12, 21] also at high temperatures. There are two time scales in the tunnelling process : i) the tunnelling time through the barrier and ii) the time *between* two consecutive tunnelling events. The latter of these is the dominant one and the tunnelling time i) is not very well defined and is assumed to be negligible [22, 23, 24]. The time between the tunnelling events ii) is large enough for the subsequent tunnelling events to be uncorrelated to each other. Therefore there is no 'memory' in the system, i.e., the current configuration of charges (state of the array) $\{n\}_i = \{n_1, n_2, \ldots, n_{N-1}\}$ completely determines the tunnelling probabilities to the $2N$ possible states. Once tunnelling through a junction has occurred, the new state $\{n\}_{i+1}$ once again serves as a starting point, and it has no knowledge of its past and how it got there. Thus, one obtains a series of states $\{n\}_0 \rightarrow \{n\}_1 \rightarrow \{n\}_2 \rightarrow \ldots$ each contributing to the total current. Each state $\{n\}$ has a probability $\sigma(\{n\})$ of existing, i.e., a sequence of $M$ tunnel events contains, on the average, $\sigma(\{n\})M$ number of states $\{n\}$ assuming that $\sigma$ has no time evolution.

Let us next focus on a particular state $\{n\}$ and junction $i$. Our state of interest is predicted to occur $\sigma(\{n\})M$ times, but in how many of these cases does the next electron tunnel through the junction $i$ to the right (or left)? The answer comes from the tunnelling probabilities per unit time (rate) $\Gamma_j^{\pm}(\{n\})$ to the left (-) and right (+) through junctions $j = 1, 2, \ldots, N$ at the state $\{n\}$. Note that for a given bias and array, $\Gamma$ depends on the configuration alone and does not have time evolution (Eq. (1)). The total rate out of the initial state $\{n\}$ is $\Gamma_\Sigma \equiv \sum_{j=1}^{N} \left[\Gamma_j^+(\{n\}) + \Gamma_j^-(\{n\})\right]$ and thus a fraction

$$f_i^{\pm}(\{n\}) = \frac{\Gamma_i^{\pm}(\{n\})}{\sum_{j=1}^{N} \left[\Gamma_j^+(\{n\}) + \Gamma_j^-(\{n\})\right]} \tag{18}$$

of $\sigma(\{n\})M$ take place through junction $i$ to the right (+) or left (-). The net amount of charge transferred forward (right) is

$$-e \cdot \sigma(\{n\}) \cdot M \cdot \left[f_i^+(\{n\}) - f_i^-(\{n\})\right]. \tag{19}$$

Calculating the net charge in this way has great benefit over the conceptually more appealing and simpler method of just following the electron tunnelling through junction $i$ and adding/subtracting the transferred charge depending on the direction of tunnelling. Counting the electrons in that way essentially simulates Eq. (18) numerically, but that is a futile effort since we know it already! To obtain the total net charge $\tilde{q}_i$ transferred[4] through junction $i$, i.e., the difference of charge to the right and left, respectively, one has to take all the $M$ configurations into account

$$\tilde{q}_i = -e \cdot \sum_{\{n\}} M\sigma(\{n\}) \cdot \left[f_i^+(\{n\}) - f_i^-(\{n\})\right], \tag{20}$$

where the summation is taken over the $M$ states $\{n\}_0 \rightarrow \{n\}_1 \rightarrow \{n\}_2 \rightarrow \ldots \{n\}_{M-1}$. Now, we still have a problem of the probabilities $\sigma(\{n\})$ since they are not known in advance. However, using the fact that, in the long run, each state is visited $M\sigma(\{n\})$ times, we can write Eq. (20) as

$$\tilde{q}_i = -e \cdot \sum_{\{n\}_S} \left[f_i^+(\{n\}_S) - f_i^-(\{n\}_S)\right], \tag{21}$$

where the summation is performed as the simulation progresses, i.e, for each configuration, one calculates the argument in Eq. (21) and adds it to the variable containing the sum up to the previous configuration. To distinguish this "dynamical" sum from the mathematical summation in Eq. (20), a subscript 'S' has been added. The probabilities $\sigma(\{n\})$ are now naturally taken care of in Eq. (21), since the more probable a state is, the more often it is visited and accounted for in the summation of Eq. (21), i.e., the probabilities $\sigma(\{n\})$ are estimated by simulation. Note that if one did not use Eq. (18) but simply counted electrons tunnelling back and forth, one would be estimating the tunnelling rates by simulation *in addition to* the probabilities

[4]Estimates of the actual quantities are distinguished by tilde (˜) above their symbols.

$\sigma(\{n\})$. This has little effect at low temperature, where thermally excited tunnelling is rare and the difference $f_i^+ - f_i^-$ is large, but at high temperature most tunnelling events are thermal and the difference $f_i^+ - f_i^-$ is small as compared to $f_i^+$ or $f_i^-$.

To calculate the current, one needs to know the time associated with the charge transfer. The probability that a given configuration $\{n\}$ is preserved for a time period $\Delta t$ is [15]

$$P(\Delta t) = \exp(-\Gamma_\Sigma \Delta t) \tag{22}$$

from which one readily obtains the average time spent in $\{n\}$

$$\Delta t(\{n\}) = \frac{1}{\Gamma_\Sigma} = \left( \sum_{i=1}^{N} \left[ \Gamma_i^+(\{n\}) + \Gamma_i^-(\{n\}) \right] \right)^{-1} . \tag{23}$$

As in calculating the charge (Eq. (21)), the total time $T$ associated with the transferred charge is obtained by dynamically summing Eq. (23) along the simulation path[5]

$$\tilde{T} = \sum_{\{n\}_S} \Delta t(\{n\}_S), \tag{24}$$

and now the current through junction $i$ is easily obtained as

$$\tilde{I}_i = \frac{\tilde{q}_i}{\tilde{T}} = -e \cdot \frac{\sum_{\{n\}_S} \left[ f_i^+(\{n\}_S) - f_i^-(\{n\}_S) \right]}{\sum_{\{n\}_S} \Delta t(\{n\}_S)}, \tag{25}$$

i.e., the nominator and the denominator in Eq. (25) are separately calculated during the simulation and, at the end, the results are divided to obtain the current. Note that the factor $M$ (Eq. (20)), the length of the simulation run, is canceled in the division, as it naturally should.

In equilibrium, the current through each of the junctions has to be the same, i.e., $I = I_1 = I_2 = \ldots = I_N$, one can average over the $\tilde{I}_i$'s and assign (arbitrary) weight $p_i$ on them, too, because

[5] Average time $\Delta t$ is an exact quantity whereas the total time $\tilde{T}$ is an estimate due to the finite sampling of the configuration space.

$$\sum_{i=1}^{N} I_i \cdot p_i = I \cdot \sum_{i=1}^{N} p_i = I, \tag{26}$$

provided that the weights are normalized: $\sum_{i=1}^{N} p_i = 1$. Due to the finite sums involved, there is no ambiguity in interchanging the summations over $i$ and $\{n\}_S$ to obtain the current from Eq. (25) as

$$\tilde{I} = \frac{\sum_{\{n\}_S} \widetilde{\Delta Q}\left(\{n\}_S\right)}{\sum_{\{n\}_S} \Delta t\left(\{n\}_S\right)}, \tag{27}$$

where we have introduced a notation

$$\widetilde{\Delta Q}(\{n\}) = -e\frac{\sum_{i=1}^{N}\left[\Gamma_i^{+}(\{n\}) - \Gamma_i^{-}(\{n\})\right] \cdot p_i}{\sum_{i=1}^{N}\left[\Gamma_i^{+}(\{n\}) + \Gamma_i^{-}(\{n\})\right]}. \tag{28}$$

By suitably choosing $p_i$ we can significantly speed up the computation in practise. To determine the desirable weights $p_i$, consider the tunnel resistances $R_{T,i}$. Tunnelling rate $\Gamma_i^{\pm}$ is inversely proportional to $R_{T,i}$ and hence low resistance implies large rates and a small relative difference between the forward and backward tunnelling rates (Eq. (28)). Therefore, because current, i.e., net tunnelling rate of electrons is the same for all junctions, small difference in rate implies high noise level, which we effectively eliminate by applying a low weight on such a junction. Hence we choose the weight as [25]

$$p_i = \frac{R_{T,i}}{R_{\Sigma}}, \tag{29}$$

although it is perfectly valid to experiment with other weights as well as long as they sum up to unity. The weight factor in Eq. (29) greatly improves the accuracy when simulating inhomogenous arrays at not that low temperatures.

Equations (23), (27), (28) and (29) present the main part of the simulation method. The tunnelling rates, $\Gamma_i^{\pm}$, are calculated by considering the energy difference $\Delta F$ before and after a tunnelling event. Let $\varphi_i$ denote the potential of the island $i$ before tunnelling and $\varphi_i'$ the potential after the tunnelling

event. The change of energy in the tunnelling event at island $i$ is given by [15]

$$\Delta F_i^{\pm} = \frac{1}{2}e\left[(\varphi_{i\pm1} + \varphi'_{i\pm1}) - (\varphi_i + \varphi'_i)\right] \quad (30)$$

where $i \pm 1$ is the island that an electron tunnelled onto from island $i$. The potentials $\varphi_i$ are calculated from the equation

$$-C_i\varphi_{i-1}+(C_i+C_{i+1}+C_{0,i})\varphi_i-C_{i+1}\varphi_{i+1} = -en_i+q_{0,i}\ ,\ i=1,\ldots,N-1 \quad (31)$$

with $\varphi_0 = V/2$, $\varphi_N = -V/2$ and $q_{0,i}$ is the background charge on island $i$. Equation (31) is general, however, and applies to nonsymmetric bias configurations, too. The tunnelling rate through junction $i$ is

$$\Gamma_i^{\pm} = \frac{1}{e^2 R_{T,i}} \frac{\Delta F_i^{\pm}}{1-\exp(-\Delta F_i^{\pm}/k_B T)} . \quad (32)$$

At each configuration $\{n_i\}$ one calculates Eq. (32) for all the $2N$ tunnelling rates and throws a weighted dice according to the $\Gamma_i^{\pm}$'s to determine the tunnelling event that *actually* takes place. This can be realized, e.g., by dividing the interval [0,1] into $2N$ segments proportional to $\Gamma_i^{\pm}$'s and choosing an evenly distributed random number $r \in [0,1]$. The segment into which $r$ lands determines the tunnelling event.

### 2.4.3 A practical method to extract $V_{1/2}$ from the conductance data

We next turn our attention to the practical determination of temperature from the measured data. In order to use arrays of tunnel junctions as thermometers, one needs a method of extracting the half width $V_{1/2}$ from the measured conductance data. Though determining $V_{1/2}$ directly from a monitor screen may be the easiest way, a less subjective and more accurate and automated procedure is clearly needed.

For shallow dips, one can fit Eq. (3) for conductance data points to obtain $V_{1/2}$. But as the dip gets deeper, the higher order terms become noticeable and the shape of the dip begins to deviate from the first order form

(cf. Fig. 5). Including more terms from the conductance series (Eq. (7)) in the fitting procedure would be most inconvenient due to the nonlinear fitting required. Instead, we perform polynomial fits of second order to the selected regions of the conductance curve around the peak, and the half width regions, respectively, and obtain the asymptotic conductance $G_T$ as an average at high positive and negative bias regions. The fits are illustrated in Fig. 7.

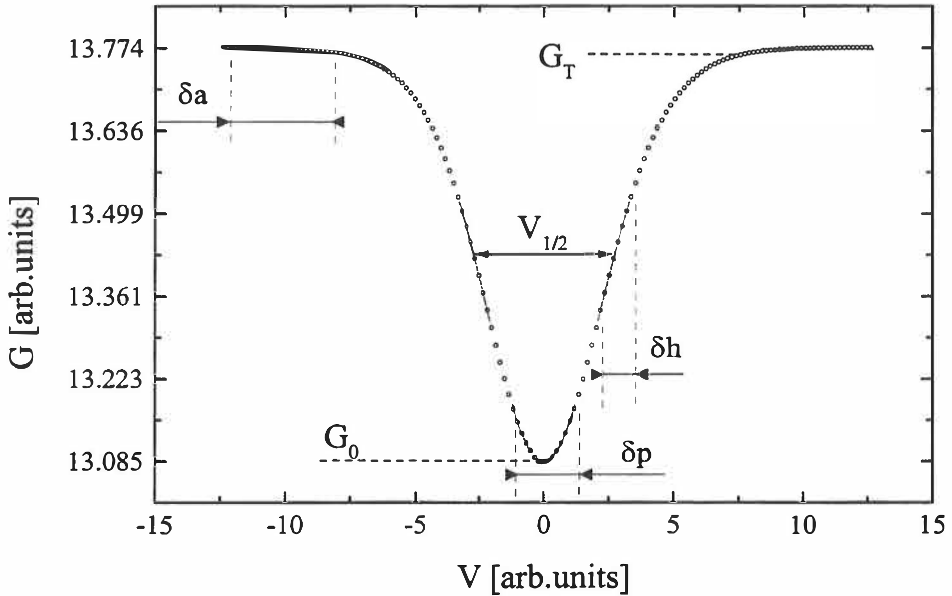


Figure 7: *Parabolic fits (solid lines) to discrete conductance points around the peak, over an interval $\delta p$, and near the half width region, $\delta h$. Far from $V = 0$, $G_T$ is obtained as an average across a region $\delta a$ (horizontal line) and the conductance at zero bias is $G_0 = G(V = 0)$.*

The algorithm of determining $V_{1/2}$ in this way is described in Ref. [P6] along with discussion about optimizing the width of each fit region in the presence of noise in the experimental conductance data. The algorithm requires relatively "clean" data with no spurious data points and to this end, we developed a filtering process to be first applied to the data. The main motivation of developing the algorithm comes from the possible application of the thermometer in an automated environment. Since Eq. (3) is inherently nonlinear, fitting data to it requires an iterative process. This needs much

more computational power than a simple parabolic fit used here. The speed originates from the fact that our procedure is linear in its parameters. We estimate that the present method is about one thousand times faster than the nonlinear fitting.

## 2.5 Experimental results

### 2.5.1 Fabrication and measurements

All the samples were fabricated by electron beam lithography using two [26, 27] or three angle shadow evaporation techniques. Most arrays were made by evaporating two layers of aluminium with oxidation in between to form a tunnel barrier out of AlOx.

The overlap area between the two layers determines the size and thus the capacitance of the tunnel junctions. In case of the thermometer, depending on the operating temperature range, the junction areas were varied between $2 \cdot 10^{-3}$ and 2 $(\mu\text{m})^2$. Figure 8 depicts the measurement geometry. One actually measures resistance versus bias curve which is easily converted into conductance. It is also possible to measure $\mathrm{d}I/\mathrm{d}V$, i.e., conductance directly. Most measurements have been made in a single ended configuration.

Measured conductances follow the expression of Eq. (3) very closely. At present, the absolute accuracy of the thermometers is about 0.3%. As an example we show in Fig. 9 data of a sample with $N = 20$ junctions at $T = 4.212$ K. Applying the method of Sec. 2.4.3 to the data of Fig. 9 yields $V_{1/2} = 40.183$ mV, whereas the calculated value is 39.499 mV by Eq. (5) with no corrections whereas the corrected value is 40.226 mV.

### 2.5.2 Physical limitations

The ratio of thermal energy $k_B T$ to the characteristic charging energy $E_C = e^2/2C$ determines whether the temperature is high or low for the thermometric operation. This would suggest that one can choose the thermometer parameters to work at any absolute temperature, given the technology to control the junction capacitance $C$. There are, however, limitations at very high and low temperatures due to material factors. The temperature that is actually measured is the electronic one, but usually one is interested in the temperature of the lattice rather than that of the electrons. This becomes a limiting factor at low absolute temperatures due to the poor coupling between

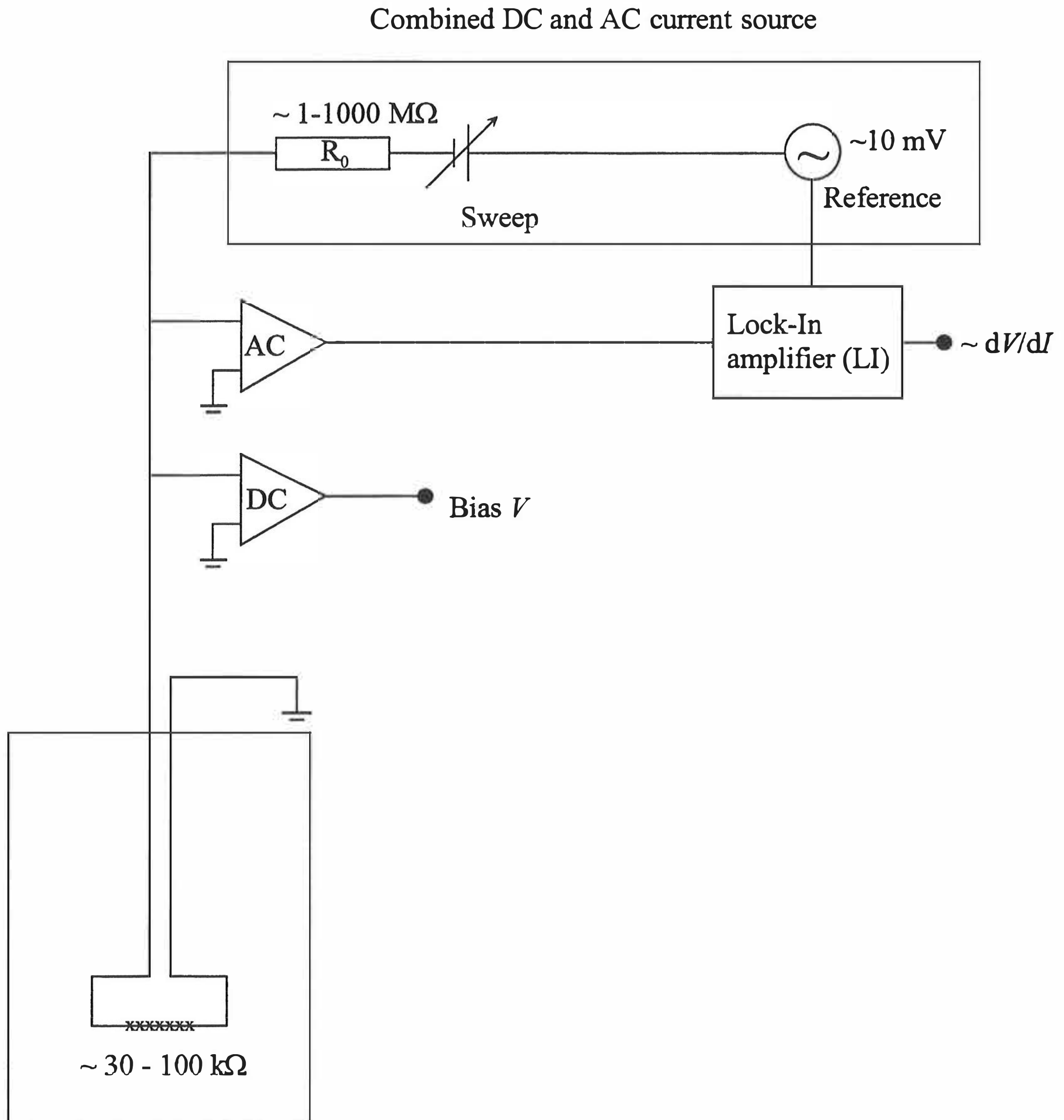


Figure 8: *A simple measurement setup. The sample array is inside a refrigerator and it is biased through a resistor $R_0$ by sweeping the voltage. Small AC voltage is added to the sweep for lock-in (LI) purposes and the actual bias voltage over the array is measured by a DC preamplifier. The output for LI is proportional to the differential resistance $dV/dI$ of the array, provided $R_0$ is much greater than $R_\Sigma$, the resistance of the array.*

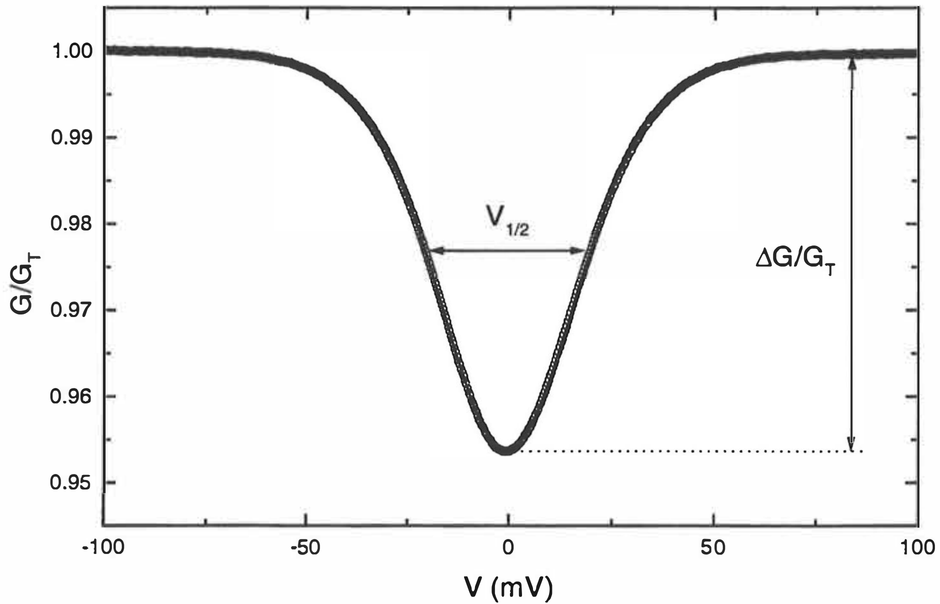


Figure 9: *An example of a measured peak ($\Delta G/G_T = 4.6$ %) of an array of $N = 20$ junctions at $T = 4.2$ K. The solid line shows the analytical result by Eq. (3).*

electrons and phonons. There is inevitably heating due to the measurement currents (DC and AC) and, hence, at low absolute temperature the electronic temperature is higher than that of the lattice due to the poor thermalization and this results in a systematic error in temperature measurement. Thermal connection between the crystal lattice of the Al island and the substrate is not a bottleneck[28].

At the high absolute temperature end, bias sweep over a wide range is required to measure the whole conductance peak. However, at high biases the tunnel barrier whose height is about 2 eV is distorted significantly from the square shaped one and this results in deviations from the simple theoretical prediction of Eq. (3) because the simple expressions of, e.g., Eq. (32) for the tunnelling rates are not strictly valid any more in the presence of "barrier suppression". This is exemplified in the figures of Refs. [P2], [29]. Fig. 10 depicts schematically the limitations.

Last, but by no means the least, property of the tunnel junction ther-

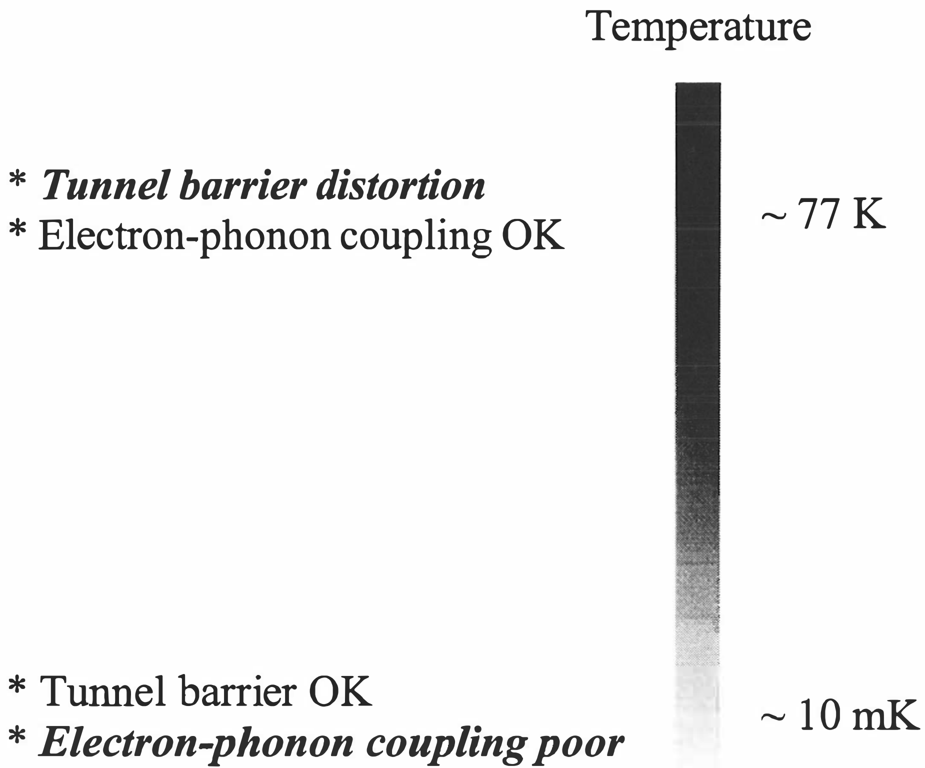


Figure 10: *Schematic illustration about physical limitations of CBT thermometry with $Al/AlO_x/Al$ junctions at high/low absolute temperatures.*

mometer is the independency of its reading on magnetic field [P3] at least up to 8 T and within 2% of reproducibility of the experiments. Measurements even at higher magnetic fields are in progress.

### 2.5.3 Solitary junctions

Unlike arrays, a solitary tunnel junction is believed to show no charging effects in the simplest picture with perfect voltage bias across. Experimentally, a significant zero bias anomaly in the form of a drop of conductance exists also in single junctions [30, 31, 32, 33]. We have developed a phenomenological model for the charging effects in a solitary junction. Due to the shortness of the tunnelling time and the remoteness of the voltage source we may assume that the bias across the junction drops at the very instant of the

electron tunnelling event. The effective circuit seen by the electron is shown in Fig. 11 where the capacitances $C_e$ result from the leads connected to the junction. The electron 'sees' length $c\tau$ of the leads, where $\tau \sim \hbar/\Delta E$ with $\Delta E = max(eV, k_BT)$ is the uncertainty time associated with the tunnelling, and, $c$ is the propagation velocity of the electromagnetic signals.

One is able to derive, at high enough $T$, a formula for the conductance [P2],[34] similar to Eq. (3), but now for single junctions. We can treat this

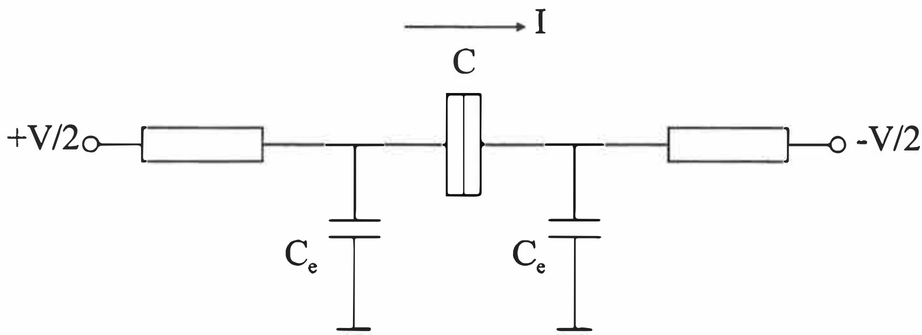


Figure 11: *Phenomenological model for charging in solitary junctions: effective circuit.*

problem also directly based on the microscopic theory reviewed in Ref. [35]. From this theory we obtain an equation for the two tunnelling rates as

$$\Gamma^{\pm}(V) = \frac{1}{e^2 R_T} \int_{-\infty}^{\infty} \gamma(\pm eV - E) P(E), \tag{33}$$

where $\gamma(x) = x/(1 - exp(-x/k_BT))$, and $P(E)$ is the probability for an electron to exchange energy $E$ with the environment in a tunnelling event. The current can now be calculated from $I = -e[\Gamma^+(V) - \Gamma^-(V)]$.

Because $P(E)$ is peaked around $E = 0$ and vanishes as $E$ tends to $\pm\infty$, we can expand the $\gamma(\pm eV - E)$ around $\pm eV$. By substituting this expansion to the formulae of current up to the first order and using the facts $\int P(E)dE = 1$ and $\int EP(E)dE = e^2/2C$ we obtain, in perfect analogy to Eq. (3)

$$G(v_S)/G_T = 1 - u_S g(v_S) \tag{34}$$

with $v_S = eV/k_BT$ and $u_S = (e^2/C_{eff})/k_BT$, where $C_{eff}$ is the capacitance seen by the junction.

## 2.6 Pumping single electrons by surface acoustic waves

### 2.6.1 Controlling single charges: metrological applications

The ability to control charges on a single electron level allows one to construct a current standard - at least in principle. Consider an array of tunnel junctions with *gates* attached in the vicinity of the islands (Fig. 1). Gates are simply metallic leads manufactured near the island producing a capacitance $C_{g,i}$ with island $i$. By applying a voltage $V_{g,i}$ to the gates through external wiring, one can *alter* the potentials of the islands.

**An electron pump** is a device that transfers single electrons one by one through the array by modulating the potentials of the islands. Triangular shaped voltage pulses applied to the successive islands form a potential well containing a single electron [36], $V_{g,i}C_{g,i} + V_{g,i+1}C_{g,i+1} = e$, which propagates from one end of the array to the other. Charge is transported even in the absence of bias voltage $V$. Given the frequency $f$ of single electron propagation through the whole array, we obtain a relation

$$I = ef. \tag{35}$$

for the current $I$. Since $f$ can be measured very accurately, Eq. (35) gives us an accurate measure of $I$, provided an accurate electron pump can be manufactured. The state-of-the-art circuits are accurate to 15 parts in $10^{-9}$ in transferring electrons [2].

**An electron turnstile** also transfers single electrons [37] one by one, but there is only one gate in the middle (see Fig. 1 with even $N$ and one middle gate only) island and finite bias voltage is required for the operation. With bias applied, the gate voltage first pulls an electron into the center island from one side and eventually, in the second half of the clock cycle, pushes the electron out of the array through the other side. Configurations where an electron resides on either halves of the array are not stable, but lead into a cascade of tunnel events, i.e., once an electron is not on the center island, it is bound to continue tunnelling toward the center island or out of the array determined by the bias and gate voltages. Eq. (35) holds also for a turnstile.

The accuracy of the pump and turnstile are degraded by cotunnelling effects, thermally activated tunnelling and possible background charge fluctuations. Increasing the number of junctions [1, 2, 36] helps to prevent the

cotunnelling problem, but long arrays are more tricky to operate. Low current level is one of the obstacles in practical realizations of Eq. (35) and cannot be arbitrarily increased by increasing the modulating frequency $f$. The characteristic cut-off frequency of electron tunnelling is on the order of $1/R_TC$, and if the frequency is $f \gg 1/R_TC$, the electron cannot follow the traveling potential well. In fact, the stochastic nature of tunnelling limits the upper operating frequency $f$ of any single charge transferring device independently of its detailed design. There is also a practical limitation for long arrays, since external wiring is needed for the gates in the electron pump. In turnstile, gates for the other islands, in addition to the center one, are needed to compensate for the nonzero background charges.

### 2.6.2 SAW pump

In the electron pump one needs external wiring for the gates which severely limits the practical maximum length of the array and makes it inconvenient to use several arrays in parallel. Parallel arrays could be used to increase the current level in the single charge transfer devices.

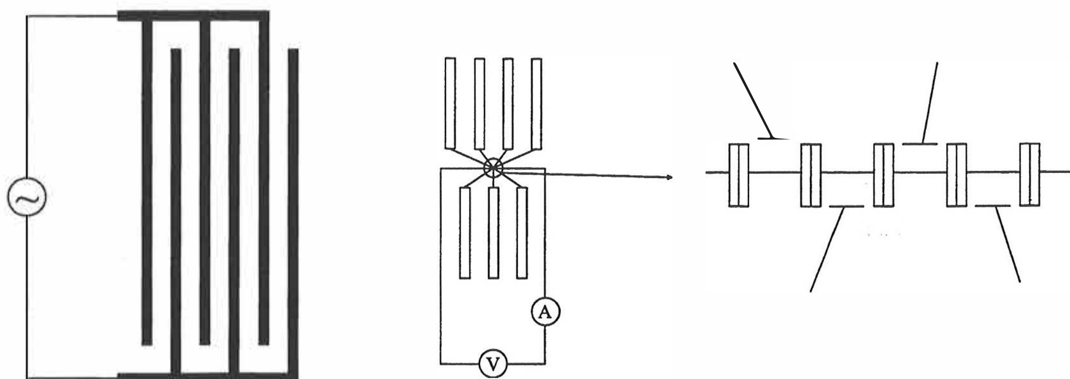


Figure 12: *Principle of the SAW measurement. Transducer on the left generates surface acoustic waves (SAW), which are picked up by large antennas near the array. The induced voltage is coupled to the islands via gates connected to the antennas.*

We have used *surface acoustic waves* (SAW) to modulate the potentials of the islands [P7]. The SAW on a piezoelectric surface, in our case GaAs, is an electroacoustic wave that can be created by interdigital transducers, see, e.g., Ref. [38]. The wavelength $\lambda$ is determined by the distance between the fingers of the transducer. By the SAW one can create ac potentials on

the islands of practically equal amplitude and well-defined phases simply by choosing the amplitude of the SAW and the ratio between $\lambda$ and the distance between the gates in the SAW field without external leads.

Experimental setup is shown in Fig. 12 and it was used to demonstrate the pumping by SAW [39]. Since the islands are quite small, the coupling of SAW through the stray capacitance $C_{0,i}$ is weak and one needs additional antennas to pick up the SAW signal.

Numerical simulations of SAW pumping were performed by adding a periodically modulated charge on each island. Now there is time evolution in the probabilities $\sigma$, tunnelling rates $\Gamma$ and thus one cannot use the accelerated version (namely, Eq. (18) for the rates) of the simulation method described earlier. To be specific, let us list the points to be taken care of:

- Due to the time dependence one has to proceed in steps of time $\Delta t$ that are small compared to the characteristic time scale in the system which, in our case, is the period of modulation $1/f$. For example, we can choose $\Delta t = 0.05/f$.

- One has to follow the single electron tunnelling events through junctions and *not* to use the average 'rate' of Eq. (18). For each junction $i$ one obtains the net charge transferred forward $\tilde{q_i}$ (like Eq. (20)) which can be averaged over the junctions $\tilde{Q}_{ave} = \left(\sum_{i=1}^{N} \tilde{q_i}\right)/N$ since there is no accumulation of charge inside the array.

- SAW modulation can be modelled as an effective time dependent charge modulation added on the islands $Q_{SAW,i}(t) = C_{g,i}V_{g,i}(t)$. Therefore, the right hand side of Eq. (31) changes to $-en_i + q_{0,i} + Q_{SAW,i}(t)$ and the potentials $\varphi_i$ are calculated using this modified equation.

- Tunnelling rates are calculated as usual from Eq. (32). At each step Eq. (22) is used to test whether a tunnelling event takes place or not, i.e., does the current configuration survive the time $\Delta t$ (a random number is needed). Time is incremented by $\Delta t$ and the possible tunnelling event taking place is realized in the same manner as before.

Note the conceptual difference between the SAW and thermometer simulation methods. In the former we have constant steps in time and during each time step a tunnelling event may or may not take place. In the latter we have 'constant' steps in configuration space, i.e., at each step a tunnelling event takes place and the corresponding step in time vary from one event to another. This approach is possible because there is no change in the physical

conditions (bias, etc.) of the array between the tunnelling events. Of course, it would be possible to have constant steps in time in this case, too, and at each step use Eq. (22) to test whether electrons tunnel or not, but this would be simply a less effective method.

SAW pump is a single charge transfer device and thus requires low temperatures for operation. It was discovered experimentally as well as by numerical investigations, that background charges are the main problem in the SAW pump. This effectively undermines the advantage of SAW, namely the wireless modulation which easily allows the use of parallel arrays to increase the current level. The piezoelectric substrate (GaAs) also has more background charge fluctuations than silicon and the charges migrate causing instability. External leads may, after all, be required for accurate operation, at least for DC compensation of charge fluctuations.

# 3 Publications

P1. J.P. Pekola, K.P. Hirvi, J.P. Kauppinen, and M.A. Paalanen, *Thermometry by Arrays of Tunnel Junctions*, Phys. Rev. Lett., **73**, 2903 (1994). https://doi.org/10.1103/PhysRevLett.73.2903

For the first time, we showed that arrays of tunnel junctions between normal metal electrodes exhibit features suitable for primary thermometry in an experimentally adjustable temperature range where thermal and charging effects compete. A universal analytic high temperature result for $IV$ and $\mathrm{d}I/\mathrm{d}V$ vs. $V$ curves of a two junction array was calculated. Experimentally the width of the conductance minimum in this regime scales with $T$ and $N$, the number of junctions, and its value (per junction) agreed with the calculated one to within 3% for large $N$ in these first experiments.

P2. Sh. Farhangfar, K.P. Hirvi, J.P. Kauppinen, J.P. Pekola, oJ.J. Toppari, D.V. Averin, and A.N. Korotkov, *One Dimensional Arrays and Solitary Tunnel Junctions in the Weak Coulomb Blockade Regime: CBT Thermometry*, J. Low Temp. Phys., **108**, (in press, 1997). https://doi.org/10.1007/BF02396821

This is a review article on the use of tunnel junction arrays for primary thermometry. In addition to the basic experimental and theoretical results, important new results of this article are the low temperature corrections to the half width and depth of the measured conductance dip beyond the linear approximation. It is also pointed out that short

arrays, single tunnel junctions in particular, show interesting deviations from the universal behaviour of the long arrays.

P3. K.P. Hirvi, J.P. Kauppinen, A.N. Korotkov, M.A. Paalanen, and J.P. Pekola, *Arrays of normal metal tunnel junctions in weak Coulomb blockade regime*, Appl. Phys. Lett., **67**, 2096 (1995). https://doi.org/10.1063/1.115090

Thermometric features of the $IV$ characteristics of one dimensional arrays of normal metal tunnel junctions were tested against inhomogeneities in the junction parameters, number of junctions in the array, and magnetic field. Arrays were found to be robust against fabrication inhomogeneities and no dependence of magnetic field was found up to 8 T with 2 % of reproducibility of the experiments.

P4. K.P. Hirvi, J.P. Kauppinen, M.A. Paalanen, and J.P. Pekola, *Primary Thermometry with Nanoscale Tunnel Junctions*, J. Low Temp. Phys., **101**, 17 (1995). https://doi.org/10.1007/BF00754557

First computer simulation studies of the effect of background charges are presented here. Inhomogeneities in the array were numerically studied by applying large deviations of junctions areas (i.e. resistances and capacitances).

P5. K.P. Hirvi, M.A. Paalanen, and J.P. Pekola, *Numerical investigation of one-dimensional tunnel junction arrays at temperatures above the Coulomb blockade regime*, J. Appl. Phys., **80**, 256 (1996). https://doi.org/10.1063/1.362813

This is my central paper, where background charge effects were studied in depth and a temperature correction vs. peak depth curve was calculated for peaks at not so high $T$ as Eqs. (3-5) require in order to be accurate enough. The simulation and data analysis methods are presented in detail.

P6. K.P. Hirvi and J.P. Pekola, *Determination of thermometric parameters from the conductance curve of a normal metal based tunnel junction array*, submitted to Comp. Phys. Commun. (1997). https://doi.org/10.1016/S0010-4655(97)00071-4

A practical method of extracting thermometric parameters from the measured conductance curve vs. bias voltage of tunnel junction array, is presented. Instead of fitting the whole theoretical conductance curve to the experiment, we perform several parabolic fits to selected bias regions. The advantage of this method lies in the simplicity and the subsequent speed of polynomial fits as opposed to the fitting of

inherently nonlinear theoretical conductance curve. Optimizing the polynomial fit procedure is discussed.

P7. A.B. Zorin, J.P. Pekola, K.P. Hirvi, and M.A. Paalanen, *Pumping of single electrons with a traveling wave*, Physica B, **210**, 461 (1995). https://doi.org/10.1016/0921-4526(94)01134-M
Surface acoustic wave was used in modulation of the potentials of the islands in an array to achieve a pumping of electrons through the array. The resulting transfer of charges should produce a DC current $I = \pm ef$ through the chain, where $f$ is the frequency of the wave and the sign of the current depends on the value of the common DC bias of the islands as well as on the direction of the wave propagation. However, a much smaller current was observed and the most harmful factor in practise was found to be the uncompensated background charges of random nature. Simulations on the effect of the background charges were made.

P8. K.P. Hirvi, T. Mäkelä, J. Pekola and M.A. Paalanen, *Economical device for measuring thickness of a thin polymer film*, Rev. Sci. Instr., **65**, 2735 (1994). https://doi.org/10.1063/1.1144609

An economic device for measuring the thickness of thin ($< 1$ $\mu$m) polymer films using three semiconductor lasers, was developed. The device has been used in measuring various dielectric coatings on silicon and glass substrates.

# 4 The author's contribution

I am responsible for all the numerical work presented in this thesis. I performed the computer simulations in [P7] studying the effect of background charges on single electron transport by surface acoustic waves. In Ref. [P1] I took part in data analysis, and in [P3] I developed a simulation program for inhomogenous arrays and studied the effect of uneven junction parameters numerically. Background charge simulations in [P4] were performed by me and most of the data of the figures were collected by me. Publication [P5] was written by me and simulations and data analysis methods were my work. Also, I wrote Ref. [P6] and performed programming and testing of the algorithm. I constructed the instrument of [P8] and verified its performance.

# References

[1] J.M. Martinis, M. Nahum, and H.D. Jensen. *Phys. Rev. Lett.*, **72**, 904 (1994).

[2] M.W. Keller, J.M. Martinis, N.M. Zimmerman, and A.H. Steinbach. *Appl. Phys. Lett.*, **69**, 1804 (1996).

[3] L.R.C. Fonseca, A.N. Korotkov, and K.K. Likharev. *J. Appl. Phys.*, **79**, 9155 (1996).

[4] P.D. Dresselhaus, L. Ji, Siyuan Han, J.E. Lukens, and K.K. Likharev. *Phys. Rev. Lett.*, **72**, 3226 (1994).

[5] K.K. Likharev and A.N. Korotkov. *Science*, **273**, 763 (1996).

[6] A.N. Korotkov, R.H. Chen, and K.K. Likharev. *J. Appl. Phys.*, **78**, 2520 (1995).

[7] L.R.C. Fonseca, A.N. Korotkov, K.K. Likharev, and A.A. Odintsov. *J. Appl. Phys.*, **78**, 3238 (1995).

[8] S.E. Kubatkin, A.Ya. Tzalenchuk, Z.G. Ivanov, P. Delsing, R.I. Shekhter, and T. Claeson. *JETP Lett.*, **63**, 126 (1996).

[9] A.N. Korotkov. *Appl. Phys. Lett.*, **69**, 2593 (1996).

[10] A.N. Korotkov, D.V. Averin, K.K. Likharev, and S.A. Vasenko. In H. Koch and H. Lübbig, editors, *Single-Electron Tunneling and Mesoscopic Devices*, page 45. Springer-Verlag, Heidelberg, 1992.

[11] A.N. Korotkov. *Phys. Rev. B*, **49**, 16518 (1994).

[12] D.V. Averin and Yu.V. Nazarov. In H. Grabert and M.H. Devoret, editors, *Single Charge Tunneling, Coulomb Blockade Phenomena in Nanostructures*, page 217. Plenum Press, New York, 1992.

[13] D.V. Averin, A.N. Korotkov, A.J. Manninen, and J.P. Pekola. *Phys. Rev. Lett.*, accepted (1997).

[14] D.V. Averin and K.K. Likharev. In B.L. Altshuler, P.A. Lee, and R.A. Webb, editors, *Mesoscopic Phenomena in Solids*, page 173. Elsevier, Amsterdam, 1992.

[15] N.S. Bakhvalov, G.S. Kazacha, K.K. Likharev, and S.I. Serdyukova. *Sov. Phys. JETP*, **68**, 581 (1989).

[16] H. Pothier. *Blocage de coulomb et transfert d'electrons un par un.* PhD dissertation, University of Paris, France, 1991.

[17] Y. Nakamura, D.L. Klein, and J.S. Tsai. *Appl. Phys. Lett.*, **68**, 275 (1996).

[18] Y. Nakamura, C.D. Chen, and J.S. Tsai. *Czech. J. Phys.*, **46**, 3339 (1996).

[19] Y. Nakamura, C.D. Chen, and J.S. Tsai. *Jpn. J. Appl. Phys*, **35**, 1465 (1996).

[20] E.S. Soldatov, V.V. Khanin, A.S. Trifonov, S.P. Gubin, V.V. Kolesov, D.E. Presnov, S.A. Iakovenko, G.B. Khomutov, and A.N. Korotkov. submitted (1996).

[21] D.V. Averin and A.A. Odintsov. *Phys. Lett. A*, **140**, 251 (1989).

[22] G.-L. Ingold and Yu.V. Nazarov. In H. Grabert and M.H. Devoret, editors, *Single Charge Tunneling, Coulomb Blockade Phenomena in Nanostructures*, page 97. Plenum Press, New York, 1992.

[23] M. Büttiker and R. Landauer. *IBM J. Res. Dev.*, **30**, 451 (1986). , and references therein.

[24] E.H. Hauge and J.A. Stovneng. *Rev. Mod. Phys.*, **61**, 917 (1989).

[25] A. Korotkov. *Private communication.*

[26] T.A. Fulton and G.J. Dolan. *Phys. Rev. Lett.*, **59**, 109 (1987).

[27] G.J. Dolan. *Appl. Phys. Lett.*, **31**, 337 (1977).

[28] J.P. Kauppinen and J.P. Pekola. *Phys. Rev. B*, **54**, 8353 (1996).

[29] J.P. Kauppinen and J.P. Pekola. In *Abstracts of Invited lectures and Contributed Papers*, page 200, St. Petersburg, 1996. Russian Academy of Sciences.

[30] L.J. Geerligs, V.F. Anderegg, C.A. van der Jeugd, J. Romkin, and J.E. Mooij. *Europhys. Lett.*, **10**, 79 (1989).

[31] P. Delsing, K.K. Likharev, L.S. Kuzmin, and T. Claeson. *Phys. Rev. Lett.*, **63**, 1180 (1989).

[32] A.N. Cleland, J.M. Schmidt, and J. Clarke. *Phys. Rev. Lett.*, **64**, 1565 (1990).

[33] P. Wahlgren, P. Delsing, and D.B. Haviland. *Phys. Rev. B*, **52**, 2293 (1995). P. Wahlgren, licentiate thesis, Chalmers University of Technology (1995).

[34] J.P. Kauppinen and J.P. Pekola. *Phys. Rev. Lett.*, **77**, 3889 (1996).

[35] G.-L. Ingold and Yu.V. Nazarov. In H. Grabert and M.H. Devoret, editors, *Single Charge Tunneling, Coulomb Blockade Phenomena in Nanostructures*, page 21. Plenum Press, New York, 1992.

[36] D. Esteve. In H. Grabert and M.H. Devoret, editors, *Single Charge Tunneling, Coulomb Blockade Phenomena in Nanostructures*, page 135. Plenum Press, New York, 1992.

[37] D. Esteve. In H. Grabert and M.H. Devoret, editors, *Single Charge Tunneling, Coulomb Blockade Phenomena in Nanostructures*, page 122. Plenum Press, New York, 1992.

[38] C. Campbell. *Surface Acoustic Wave Devices and Their Signal Processing Applications*. Academic, San Diego, 1989.

[39] J.P. Pekola, A.B. Zorin, and M.A. Paalanen. *Phys. Rev. B*, **50**, 11255 (1994).